Multi-step creep tests of notched beams of silver fir (Abies alba) at different initial moisture contents

Arthur Bontemps, Rostand Moutou Pitti, Eric Fournely, Gaël Godi, Joseph Gril

Construction and Building Materials 425 (2024) 136026

Contents lists available at ScienceDirect

Construction and Building Materials

journal homepage: www.elsevier.com/locate/conbuildmat

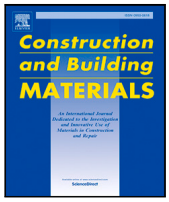

Multi-step creep tests of notched beams of silver fir (*Abies alba*) at different initial moisture contents

Arthur Bontemps [a,b,*], Rostand Moutou Pitti [a,c], Eric Fournely [a], Gaël Godi [a], Joseph Gril [a,d]

[a] Clermont Auvergne Université, CNRS, Clermont Auvergne INP, Institut Pascal, 63000, Clermont-Ferrand, France
[b] Université de Lyon, ECAM LaSalle, LabECAM, 40 Montée Saint Barthélémy, 69321, Lyon Cedex 05, France
[c] CENAREST, IRT, BP 14070, Libreville, Gabon
[d] Université Clermont Auvergne, INRAE, PIAF, 63000, Clermont-Ferrand, France

ARTICLE INFO

Keywords:
Multi-step creep tests
Relative compliance calculation
Green wood
Silver fir
Notched beams
Crack propagation
Beam theory

ABSTRACT

Silver fir is an important species for French timber engineering industry but its application faces drying issues. This paper presents the results of creep and ramp-loading bending tests on full-scale silver fir notched beams at different initial moisture contents. Initial moisture content showed no discernible impact on instantaneous maximum force, while dynamic compliance appeared to be proportional to this force, possibly due to the dowelling effect. Beam-theory equations are solved using finite differences with crack propagation assimilated to a height reduction, providing an estimation of the compliance and that total deflection primarily results from creep rather than crack. No correlation is observed between the maximum relative compliance and the initial moisture content. Besides this maximum value never reaches the deformation factor for serviceability design in Eurocode 5, suggesting oversizing for green wood. The discrepancy between experimental and theoretically derived crack openings highlights limitations in traditional beam theory, especially concerning fracture mechanics analysis and non-linear effects. For all tests upward crack trajectories towards compression zone are observed and physically discussed. These findings contribute to a better understanding of the mechanical behaviour of wood, particularly regarding creep and crack propagation, with implications for structural design and material characterisation.

1. Introduction

Silver fir (*Abies alba*) is an important species for European wood industry and accounts for 8% of the French forest [1]. Its wood is mainly used in timber construction but is currently facing drying issues due to wetwood in Auvergne-Rhône-Alpes region [2]. Understanding and predicting the mechanical behaviour of green or partially dried wood could promote the industrial development of new construction techniques. Traditional carpentry, made with undried wood for many centuries, could inspire the design of agricultural buildings or historical structures restoration. However, constraints imposed on buildings construction must be considered. Indeed, Eurocode 5 penalises wood that may dry under loading, e.g. green wood in service class 3. k_{def}, the deformation factor for serviceability design, is increased by 1 in that situation [3]. That choice is justified to account for mechano-sorptive effect resulting from drying under loading [4]. However, creep of green timber structural elements is difficult to quantify as it depends on several factors: temperature, relative humidity, initial mechanical properties or physical ageing [5,6]. Increasing the temperature or the relative humidity accelerates creep [7,8]. The initial mechanical properties are strongly correlated with density, grain angle, micro-fibril angle (MFA) or knots' size [9]. These anatomical parameters influence the stress repartition between the cell wall and the wood fibers, and these two elements have a different creep behaviour [10]. Studies on the long-term mechanical properties of green wood have been realised mainly on small clearwood samples under controlled environments [10–13]. Although many studies have demonstrated that the moisture content (MC) accelerates creep [14], few have examined the mechanisms at work at large-scale timber beams in realistic sheltered-outdoor environment. In such conditions some difficulties arise: (i) MC variations under loading imply a mechano-sorptive effect that greatly accelerates creep [7]; (ii) micro-cracking due to shrinkage-swelling cause local damage associated with stress concentration and material properties variations, these latter impacting creep behaviour [15]; (iii) macroscopic flaws such as knots also alter local mechanical properties or create stress concentration; (iv) micro-fibril angle (MFA) may varies along the beam.

* Corresponding author at: Clermont Auvergne Université, CNRS, Clermont Auvergne INP, Institut Pascal, 63000, Clermont-Ferrand, France.
E-mail addresses: arthur.bontemps@uca.fr (A. Bontemps), rostand.moutou_pitti@uca.fr (R. Moutou Pitti), gael.godi@uca.fr (G. Godi), joseph.gril@uca.fr (J. Gril).

https://doi.org/10.1016/j.conbuildmat.2024.136026
Received 24 October 2023; Received in revised form 21 March 2024; Accepted 26 March 2024

Nomenclature

Abbreviations

BVP	Boundary value problem
I.C.	Initial conditions
JCSS	Joint Committee on Structural Safety
LDT	Linear displacement transducer
LVDT	Linear variable differential transducer
MC	Moisture content [%]
MOE	Modulus of elasticity [GPa]
ODE	Ordinary differential equation

Notations

$\underline{\underline{X}}$	Tensor X of order 2
$\underline{X}$	Tensor X of order 1
X^*	Apparent X
X^d	Dynamic X
X_0	Initial value of a time evoluting X
X_l, X_r	X values on the left and right sides, respectively
X_z	X value around the z axis
X_c	Corrected value of X
X_{exp}, X_{fd}, X_m	X values measured experimentally, calculated using finite difference method and modelled by an approximated equation, respectively
X_{max}	Maximum value reached for X
X_{rel}	Relative X
S_{ij}	Beam number

Variable names

ΔH	Height variation [mm]
Δx	Space step in the meshed beam [mm]
ρ_{BD}	Basic density [kg m^{-3}]
σ, ϵ	Axial stress and strain in the central zone of the beam
$\underline{\underline{A}}, \underline{b}$	Matrix and vector of 3-points centered scheme for finite difference resolution
A_{crack}	Part of the deflection explained by crack propagation [%]
C_O, C_L, C_H	Respectively crack opening, crack length and crack height [mm]
e, H, L, L_N	Respectively beam's thickness, height, length and notch length [mm]
E_S^d	Basic specific modulus [(Mm)^2 s^{-2}]
F	Applied force [kN]
$f_{crack}, f_{uncrack}$	Geometrical functions relating J^* and U_c for a given crack trajectory and for an uncracked beam, respectively
G	Shear modulus [GPa]
I	Second moment of inertia [mm^4]
J	Compliance [(MPa)$^{-1}$]
k_v	Notch reduction factor
k_{def}	Deformation factor for serviceability design
L_{trach}, D_{trach}	Tracheid length and diameter, respectively [mm]
M	Bending moment applied [N mm]
m_{od}	Oven-dry mass [kg]
N	Number of meshed points
p	Slope of the load–displacement curve [N mm^{-1}]
T, RH	Respectively temperature [K] and relative humidity [/]
U_c	Central deflection [mm]
V_g	Beam's volume in green state [m^3]

This paper presents the results of an experimental campaign on full-scale notched beams of silver fir wood at different initial moisture contents. This is in a direct continuity with a previously published study on a similar experimental campaign [16]. Notched beams are chosen because they represent assembly problematics, e.g. stress concentration and load-carrying capacity reduction. In addition to the study of wood creep, that experimental campaign therefore also investigates fracture mechanics of wooden structural elements. That kind of beam was widely studied due to their relevance in timber engineering, leading to the possibility of designing notched beams in European standards [17], using the notch reduction factor k_v [3]. In practice, it is strongly recommended to avoid notches or to add reinforcements [18]. However, notched beams are still a good subject for timber engineering research as it may couple creep and fracture mechanics [15]. This research distinguishes itself due to its focus on large-scale timber beams in realistic sheltered-outdoor environments, which closely mirrors the conditions encountered in civil engineering structures.

The experimental campaign consists in free vibration and basic-density measurements, ramp-loading bending tests in laboratory conditions and creep tests in outdoor conditions. Analysis uses beam theory, finite difference method and linear viscoelasticity to take into account crack propagation and creep. Raw results are presented, and then creep design of wooden structures is discussed.

2. Material and methods

2.1. Non-destructive examinations

The material consists in a batch of 30 notched beams from local silver fir at structural element scale, see Fig. 1. Such notches at half-height were designed to ensure failure by fracture from the notch instead of bending failure [16]. Therefore, it allows to trigger crack propagation on the desired location.

Most of the batch is flatsawn lumber (21/30), as shown in Fig. 1, while the rest is riftsawn. The batch has been received in green wood state and characterised by non-destructive examination. Beams are referenced S_{ij}, $_{ij}$ indicating the beam number.

2.1.1. Natural vibration tests

The BING© [19] method has been used to measure the dynamic longitudinal modulus of elasticity (MOE) and shear modulus G^d. It consists in measuring the frequency spectrum of free vibrations of a beam and calculating the stiffness properties using the eigen frequencies. This test was realised before notching the beams. The range of results is given in Table 1. G^d is the dynamic shear modulus in the longitudinal-tangential plane as the beams are plain sawned lumber. The distribution is determined using the maximum p-value between Shapiro test of the variable and of the logarithm of that variable, if p-value is above 0.05. The coefficient of variation, CV, defined as the ratio of the standard deviation to the mean, and the log-axial distribution comply with the probabilistic proposition of the Joint Committee on Structural Safety (JCSS) [20]. The mean MOE also complies with the estimated value from Cirad institute [21], at 11.75 GPa for green silver fir.

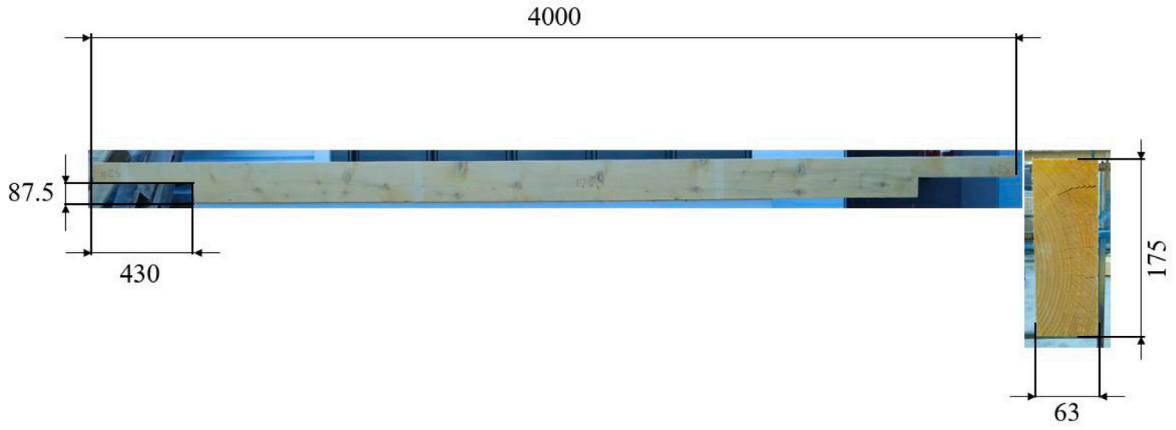

Fig. 1. Beam's dimensions (mm) from plain sawn lumber.

Table 1
Free vibration results. CV: coefficient of variation.

	MOE [GPa]	G^d [GPa]
Minimum	7.54	0.451
Maximum	16.34	0.672
Mean	11.01	0.553
CV	0.2	0.1
Distribution	Log-normal	Log-normal

Table 2
Basic-density measurements, MC at receipt and E_S^d computations.

	MC [%]	ρ_{BD} [kg m^{-3}]	E_S^d [Mm^2 s^{-2}]
Minimum	25.1	333	21.49
Maximum	117.5	430	40.84
Mean	60.3	379	28.9
Coefficient of variation	39.7	0.07	0.16
Distribution	Log-normal	Normal	Log-normal

2.1.2. Basic-density measurements

A thin slice of each beam where the green volume V_g and the ovendried mass m_{od} were measured allowed to calculate the basic density as $\rho_{BD} = (m_{od}/V_g)$. The basic density is supposed to be an intensive property, hence the same for the thin slice and for the rest of the beam. As the beams were received in green wood state, their initial volume was V_g and the basic density allows to compute m_{od} of each beam and thus the moisture content at each weighing. Finally, the basic specific modulus is computed as $E_S^d = (\text{MOE}/\rho_{BD})$. The results are given in Table 2.

The unit of E_S^d is Mm^2 s^{-2} as it is the square of the sound speed propagating in the material [22]. The distribution of ρ_{BD} follows the probabilistic proposition of the JCSS [20] and the mean value complies with the literature for silver fir [23]. It is observed that the initial MC is highly heterogeneous, from 25.1% to 117.5%, suggesting that some beams were carrying wetwood.

2.1.3. Repartition

The experimental campaign was divided into 4-points bending tests with incremental imposed displacement to study the maximum force versus MC, and 4-points bending creep tests to study the long-term mechanical evolution in outdoor conditions. Both tests were realised on beams at different initial MCs. For the creep tests 6 beams were loaded in Spring-Summer 2021, 6 in Autumn-Winter 2021–2022 and 6 in Spring-Summer 2022. Fig. 2 shows their repartition regarding their mechanical properties (E_S^d and ρ_{BD}). The whole ranges of mechanical properties have been tested at different initial MCs, as the specific basic modulus influences creep of wood [24].

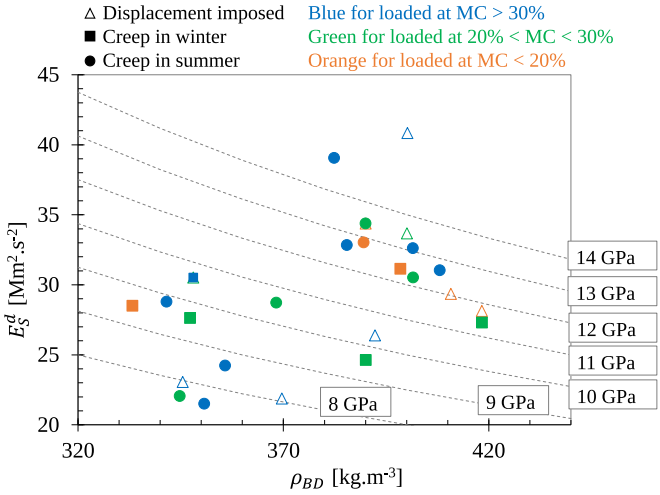

Fig. 2. Beam's repartition plotted with specific modulus (E_S^d) as a function of basic density (ρ_{BD}). Filled circle: creep test in Summer; filled square: creep test in Winter; empty triangle: ramp-loading test. Colours indicate initial moisture content (MC). Iso-modulus curves are added in grey dashed lines. (For interpretation of the references to colour in this figure legend, the reader is referred to the web version of this article.)

2.2. Bending tests

2.2.1. Ramp-loading

Displacement-controlled tests were performed in 4-points bending to correlate the maximum force with the initial MC and mechanical characteristics. The experimental set-up complies with the norm NF EN 408+A1 [25] and is represented in Fig. 3. The central deflection U_c and the crack openings on the "left" and on the "right" (respectively C_{Ol} and C_{Or}) are measured using linear displacement transducers (LDT). The applied load is measured using two load cells.

2.2.2. Multi-step creep tests

The creep tests aimed at studying the long-term mechanical behaviour of wood at different initial moisture contents. The experimental set-up, shown in Fig. 4, was in outdoor semi-sheltered conditions (i.e., sheltered from the rain but partially from solar radiation). The load was applied using m_0 = 325 kg waterproofed concrete blocks, and when possible incremented by 30 kg every month for 5 months and then every day, so that the duration of the tests never exceeded 7 months. The mass ratio $m(t)/m_0$ as a function of time is presented in Fig. 5.

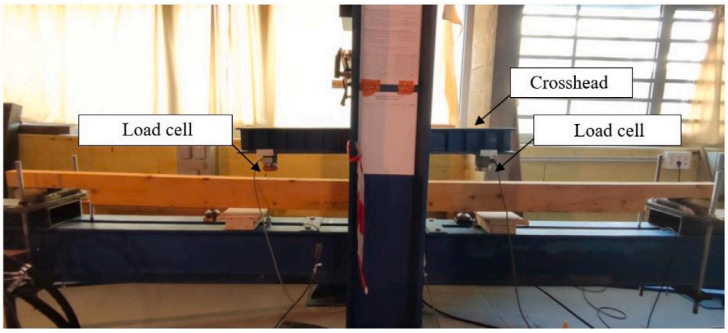

(a) Picture of a ramp-loading bending test.

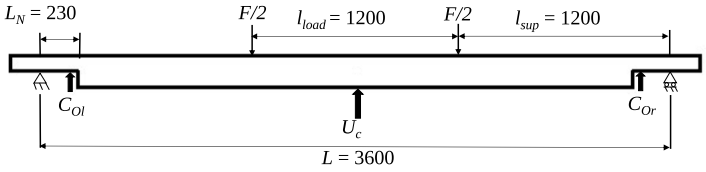

(b) Positions of measurement devices (mm).

Fig. 3. Experimental set-up of a ramp-loading test.

For central beams (Fig. 4(a)), the load increment was possible only if one of the adjacent beams had previously reached failure. Therefore, they were multi-step creep tests.

Linear variable differential transformer (LVDT) sensors were used to measure the central deflection $U_{c,exp}$. A weather station close to the tests recorded temperature (T) and relative humidity (RH). A marker-tracking technique developed for these tests was used [26]. The relative displacement between markers allowed to measure the variation of beam's height due to shrinkage-swelling (ΔH), crack opening (C_O), crack length (C_L) and height (C_H) of the observed tip, Fig. 4(c). Markers are placed on both notches, called left and right, so that indexes l and r represent the means of the two faces on left and right sides, respectively. ΔH measurements are used to correct the second moment of inertia I_z and the central deflection as the beam is notched, see Eq. (1):

$$U_{c,c}(t) = U_{c,exp}(t) - \frac{\Delta H(t)}{2} \tag{1}$$

2.2.3. Initial deflection in creep tests

An instantaneous central deflection of the creep tests was estimated by considering the central deflection at 1 min U_c^0, so that viscous effect has a similar impact to ramp-loading tests. This was calculated by the following process:

1. Determine loading duration Δt and time $t_0 = \Delta t/2$, see Fig. 6(a);
2. Plot central deflection as a function of $\log(t - t_0)$, see Fig. 6(b);
3. Focus in the region $10 \times \Delta t$ to $10 \times \Delta t + 1$ h, and the response should be linear or parabolic;
4. Apply a linear or second order polynomial regression (Fig. 6(c)), the equation then allows to compute the deflection at the desired time, here at 1 min corresponding to $\log(t - t_0) = 1.78$ if t is expressed in seconds.

2.2.4. Bending analysis

When setting the right boundary conditions the deflection of a beam leads to a simple boundary value problem (BVP) of an ordinary differential equation (ODE), resolvable analytically Appendix. Consider J the compliance, $I_z(x)$ and $M_z(x)$ respectively the second moment of inertia and the bending moment about z axis, U the deflection and x the beam's neutral axis. If J is assumed independent from the position, and the local effect of stress concentration at crack tip is neglected, it is possible to consider a crack propagation only as a height reduction, leading to a variable $I_z(x)$ evolution. As crack propagation is almost always different between the two notched-beam ends, this is an asymmetrical problem that must be resolved separately for each individual, depending on its crack trajectory. To overcome such tedious resolution, a numerical formulation using finite difference method (FDM) is proposed Appendix.

The isostatic beam in 4-points bending with its bending moment evolution is represented in Fig. 7. Noting $(\underline{C_{Ll}}, \underline{C_{Hl}})$ the couple (crack length, crack height) on the left and $(\underline{C_{Lr}}, \underline{C_{Hr}})$ on the right, the example shows an asymmetrical crack propagation after loading. All $\underline{C_L}, \underline{C_H}$ are vectors containing all previously measured crack tip positions. The beam is meshed in N points spaced by a constant Δx, as indicated in Fig. 7.

Considering the former measurement of C_H and ΔH (Fig. 4(c)), beam's height can be calculated as $H(x) = (H_0/2) + \Delta H - C_H(x)$ in the cracked region, C_H being positive if the crack rises and negative otherwise.

Essentially the FDM model uses the crack trajectory ($\underline{C_{Ll}}, \underline{C_{Hl}}, \underline{C_{Lr}}, \underline{C_{Hr}}$) to calculate the function relating the apparent compliance J^*, the applied force F and the central deflection U_c. This function called f_{crack} can be computed such that: $f_{crack} = U_{c,fd}/(J^*_{fd} \times F_{fd})$, with the deflection $U_{c,fd}$ obtained by the FDM resolution using unit values for J^*_{fd} and F_{fd}. f_{crack} is a purely geometrical function that can then be applied for an experimental estimation of an apparent compliance J^*_{exp} such that $J^*_{exp} = U_{c,c}/(f_{crack} \times F_{exp})$. The inputs and outputs of the overall resolution are presented in Fig. 8.

For an uncracked but notched beam, an analytical relation between the MOE and U_c was derived considering Timoshenko beam theory [16]. Noting $p = \Delta F/\Delta U_c$ for ramp-loading test and $p = F/U_c^0$ for creep test, the mentioned formulae are used for instantaneous calculation of the MOE.

The maximum axial stress (i.e., at $H/2$ of the neutral axis) can also be calculated using the strength of material, as shown in Eq. (2):

$$\sigma_{max}(t) = \frac{F(t).L}{e.H^2(t)} \tag{2}$$

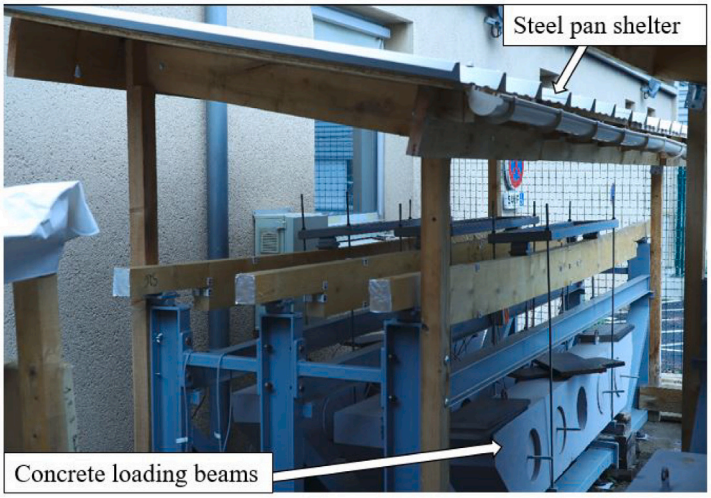

(a) Picture of three loaded beams.

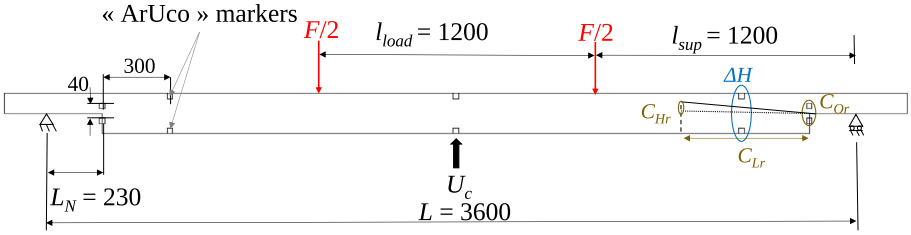

(b) Positions of measurement devices (mm).

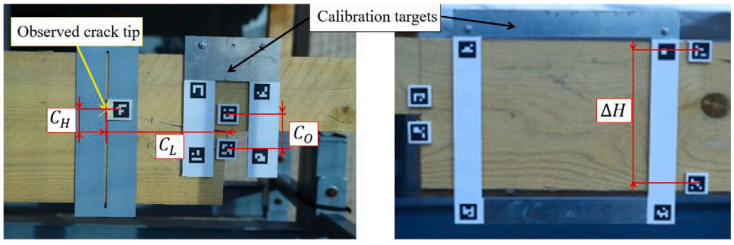

(c) Illustration of C_O, C_L, C_H measurements and height variation caused by shrinkage-swelling using relative distances between marker. Calibration targets are used for homography calculation [26].

Fig. 4. Experimental set-up of creep tests.

2.2.5. Creep analysis

The compliance J is the physical quantity that describes creep evolution. At high level of stress and in a variable environment, wood has a poorly predictable time-dependent compliance. The applied load reaches at most 700 kg, leading to a maximum axial stress in the central part of the beam of about 13 MPa.

Compared to the compressive strength of defect-free softwood that is at least 50 MPa [27], it can be considered that the linearity limit is not exceeded [28]. One might think that it is a high level of stress compared to the strength assumed by Eurocode 5 [29], but the latter considers that failure is caused by flaws that significantly reduced the local resistance. In addition, assuming that for each separate season (here, Summer and Winter), the overall tendency is a linear viscoelastic behaviour, and the compliance is an increasing function of time. In such assumptions, the superposition principle applies and the strain is defined by Eq. (3):

$$\epsilon(t) = \sum_{i=0}^{N} J(t - t_i).\Delta\sigma_i \tag{3}$$

where $\epsilon(t)$ is the axial strain evolution and $\Delta\sigma_i$ the ith number of axial stress increase, with $\Delta\sigma_0$ the initial stress. In such multi-step creep test, it is impossible to obtain $J(t)$ but rather the apparent compliance, as defined in Section 2.2.4, such as Eq. (4).

$$J^*(t) = \frac{\epsilon(t)}{\sigma(t)} = \frac{\sum_{i=0}^{N} \Delta\sigma_i.J(t - t_i)}{\sum_{i=0}^{N} \Delta\sigma_i} \tag{4}$$

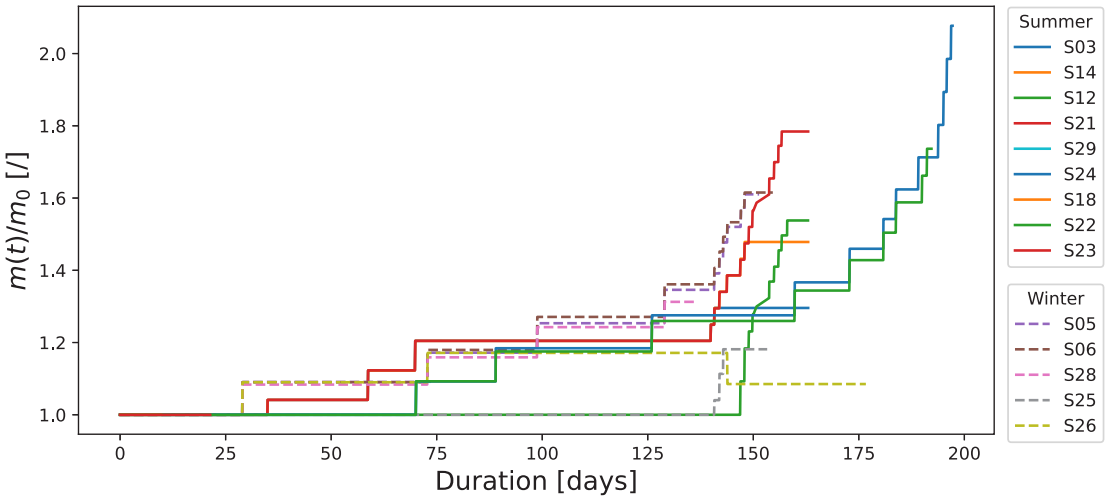

Fig. 5. Evolution of the mass ratio $m(t)/m_0$ as a function of the duration of the tests.

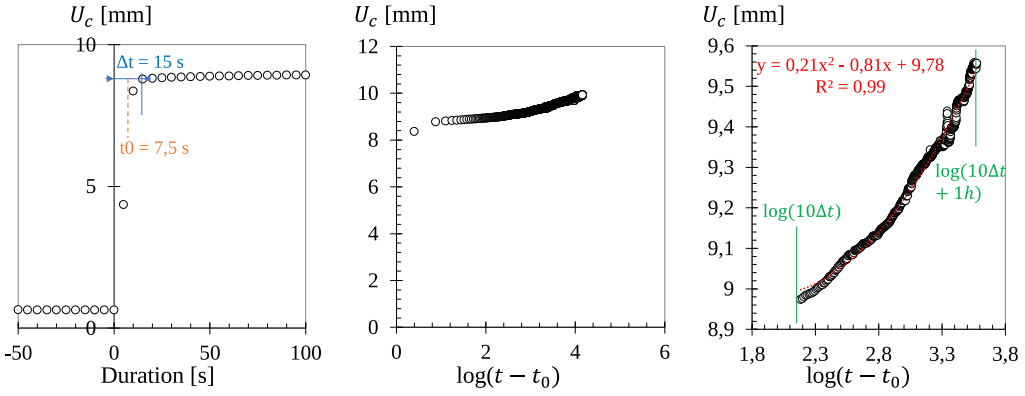

(a) Determine load duration Δt and half-duration t_0 .

(b) Plot central deflection U_c as a function of $\log(t - t_0)$.

(c) Polynomial regression skipping the beginning of the load.

Fig. 6. Calculation of U_c^0.

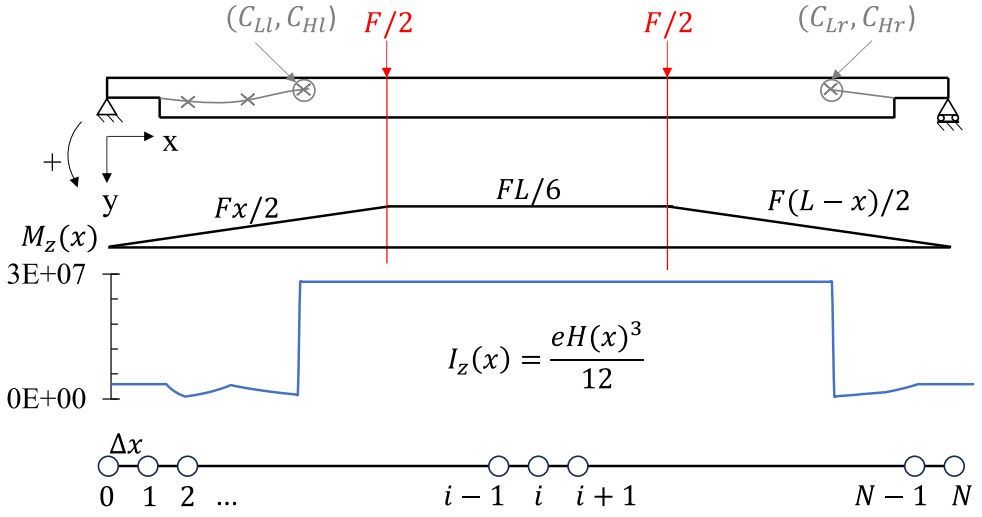

Fig. 7. 4-points bending test on an asymmetrically cracked notched beam, with its bending moment evolution and meshed definition.

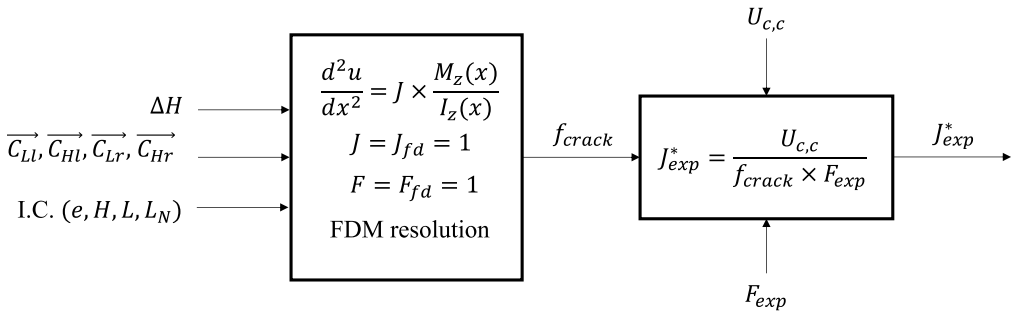

Fig. 8. Inputs and outputs of the FDM resolution of an asymmetrically cracked beam using beam theory. I.C. means Initial Conditions.

However, as $\sigma(t)$ and $J(t)$ are the increasing functions of time, Inequality (5) can be noted:

$$\epsilon(t) < \sum_{i=0}^{N} J(t).\Delta\sigma_i = J(t).\sigma(t) \tag{5}$$

That leads to Inequality (6):

$$J^*(t) < J(t) \tag{6}$$

This says that the compliance is underestimated if computed using $\epsilon(t)/\sigma(t)$ because the time elapsed since a load increase is less than the time elapsed since the start of the test, and the creep slows down with time. Therefore, the upcoming results do not represent the exact compliance J but an apparent J^*.

3. Results

3.1. Instantaneous response

3.1.1. Comparison with non-destructive examination

The approach proposed in [16] allows computing the MOE using $\Delta F/\Delta U_c$ for a notched beam, considering Timoshenko beam theory. The ramp-loading tests never exceeded 30 min and the mechanical response is hence considered instantaneous. The slope of the force–displacement curve before the first crack is used as $\Delta F/\Delta U_c$. For the creep tests, the former U_c^0 and the applied force are used.

The inverse of the MOE is considered as the initial compliance J_0. If the initial MC is below 30% ($1/J_0$) is corrected by 0.15 GPa/% [30] as J_0^d is supposed to have been measured in green state, Eq. (7) :

$$\frac{1}{J_{0,c}} = \frac{1}{J_0} + 0.15 \times (\mathrm{MC} - 30) \tag{7}$$

where $J_{0,c}$ is the corrected value of J_0. The comparison between the instantaneous results and the dynamic J_0^d is given in Fig. 9.

It is observed that in most cases $J_{0,c}$ exceeds J_0^d. The same hierarchy was observed by Nziengui with around 20% of difference [16]. Firstly, J_0 was measured on notched beams and J_0^d on unnotched beams. Stress concentration in the notch leads to a non-linear mechanical effect that is not taken into account in the equation derived by Nziengui [16]. Furthermore, changing the geometry of a heterogeneous material like wood changes the average value of its properties. Secondly, there is an intrinsic difference between the dynamic and static compliances: for instance, a value of ($1/J_0^d$) being 4% higher than ($1/J_0$) has been reported for tropical woods covering a wide range of density [31].

3.1.2. Maximum force reached

The maximum force reached during the ramp-loading tests is plotted as a function of J_0^d (Fig. 10(a)) and MC (Fig. 10(b)).

47% of the variance of F_{max} is explained by $J_{0,d}$. It was observed afterwards that the strongest beams were those with knots close to the notch, acting as reinforcement. Knots increase the compliance due to grain angle variation, but may increase the maximum force when fracture mechanics is involved. This is explained in the literature as the dowelling effect [15].

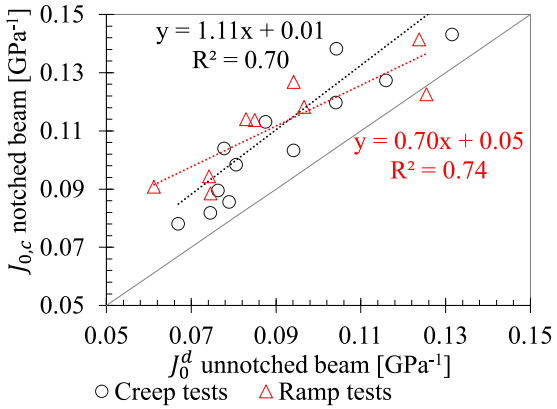

Fig. 9. Comparison between the dynamic and static $J_{0,c}$ measured on unnotched and notched beams, respectively J_0^d and $J_{0,c}$. Linear regressions are added both for creep and ramp-loading bending tests with their respective colours (red triangles for ramp-loading tests and black circles for creep tests). Bisector $y = x$ is also added in grey. (For interpretation of the references to colour in this figure legend, the reader is referred to the web version of this article.)

No correlation is observed between the instantaneous F_{max} and initial MC of the tests (Fig. 10(b)), as the drying process is too slow to have an impact for a 30 min test.

It is worth noting that a multi-step creep test is equivalent to a force-controlled ramp-loading bending test where the loading is increased much more slowly than in laboratory conditions. As creep occurs for a very slow stress-imposed test, the maximum force reached is reduced and is no more correlated to the compliance. Indeed, it is widely influenced by the environment, the initial moisture content and the viscoelastic properties of the beam.

3.2. Delayed response

Some beams failed before the initial mass m_0 was completely applied, but some reached a mass ratio above 2 (S24). It illustrates the wood variability, since such differences are caused by knots positions, growth stress cracks, initial mechanical properties, etc. As example, raw results for beam S29 loaded in summer 2022 are presented in Fig. 11. Crack propagation and shrinkage-swelling events are shown. The evolution of experimental relative compliance $J^*_{rel,exp} = (J^*_{exp} - J_0)/J_0$ is plotted as a function of time in Fig. 12. Creep tests in summer 2021 and 2022 are plotted separately from creep tests in winter 2021–2022. Hotter and drier season leads to creep acceleration and favourable conditions for crack propagation, resulting in a faster $J^*_{rel,exp}$ evolution.

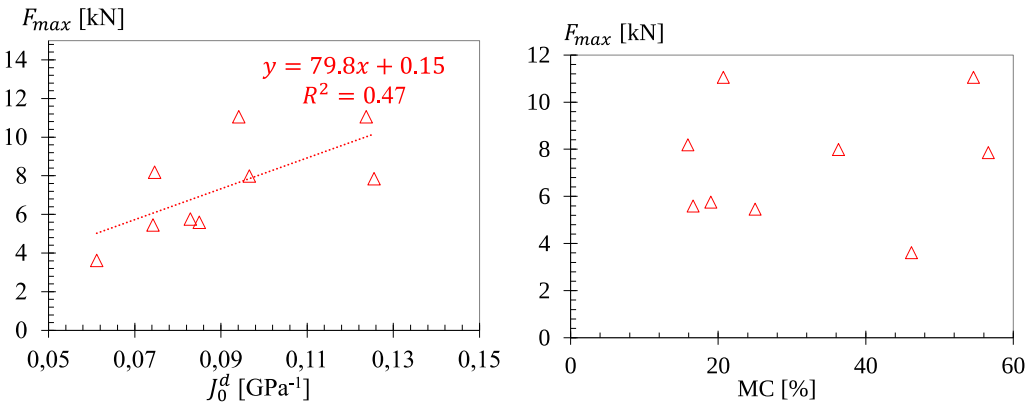

(a) Maximum force as a function of J_0^d. (b) Maximum force as a function of MC.

Fig. 10. Maximum force reached for the ramped tests.

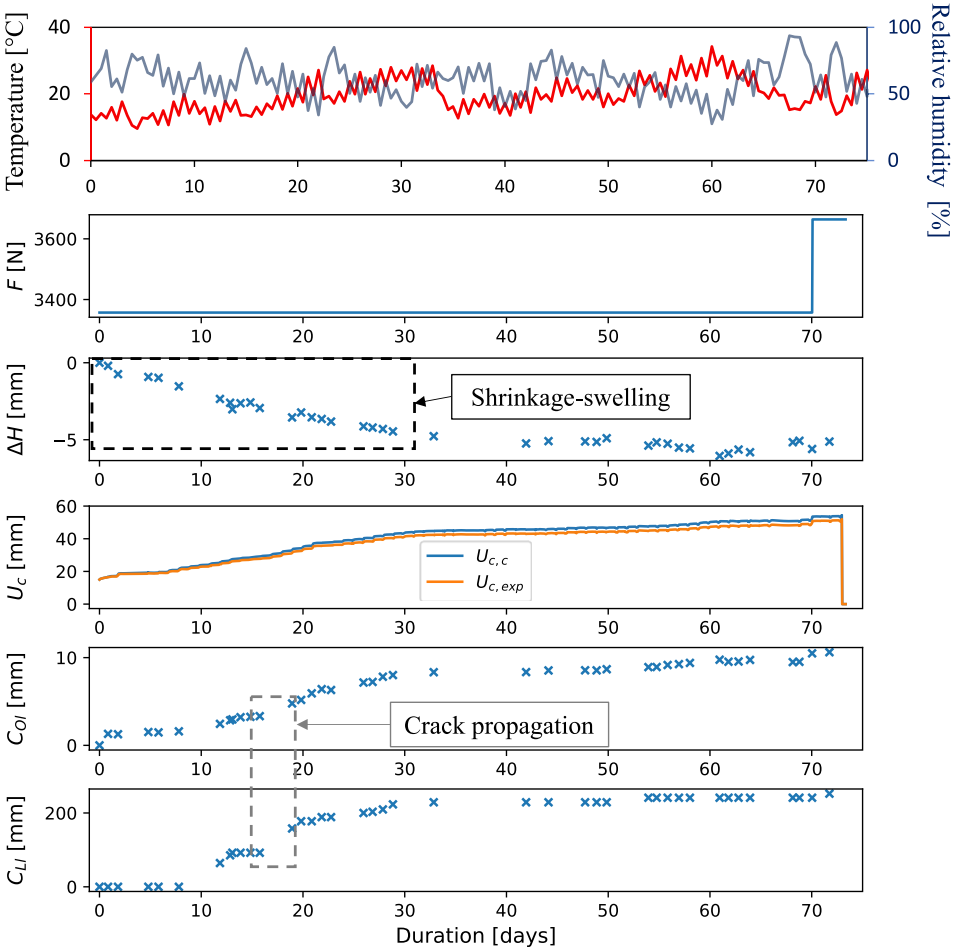

Fig. 11. Example of raw results on beam S29 loaded in summer 2022. From top to bottom : temperature and relative humidity, applied load, height variation mostly caused by shrinkage-swelling, central deflection with and without correction (Eq. (1)), crack opening and crack length on the left side. Third, fifth and sixth plots come from marker tracking measurements thus are scattered.

Creep in winter seems also smoother than in summer. Fluctuations are caused by environmental variations, crack propagation and load increase, see Fig. 13.

Load increase is easy to identify as the precise moment is known. Consistently with Inequality (6), J^* decreases when load increases. Indeed, consider that strain has an elastic and a viscoelastic contribution so that $\epsilon(t) = \epsilon_0 + \epsilon_t$, and $t_{\Delta\sigma_1}$ the time at which the 1st-load increased is applied and involves a $\Delta\sigma_1$ and $\Delta\epsilon_1$, it yields Eq. (8):

$$J^*(t^-_{\Delta\sigma_1}) = \frac{\epsilon(t^-_{\Delta\sigma_1})}{\sigma(t^-_{\Delta\sigma_1})} = \frac{\epsilon_0 + \epsilon_t}{\Delta\sigma_0} \quad \text{and} \quad J^*(t^+_{\Delta\sigma_1}) = \frac{\epsilon(t^+_{\Delta\sigma_1})}{\sigma(t^+_{\Delta\sigma_1})} = \frac{\epsilon_0 + \epsilon_t + \Delta\epsilon_1}{\Delta\sigma_0 + \Delta\sigma_1} \tag{8}$$

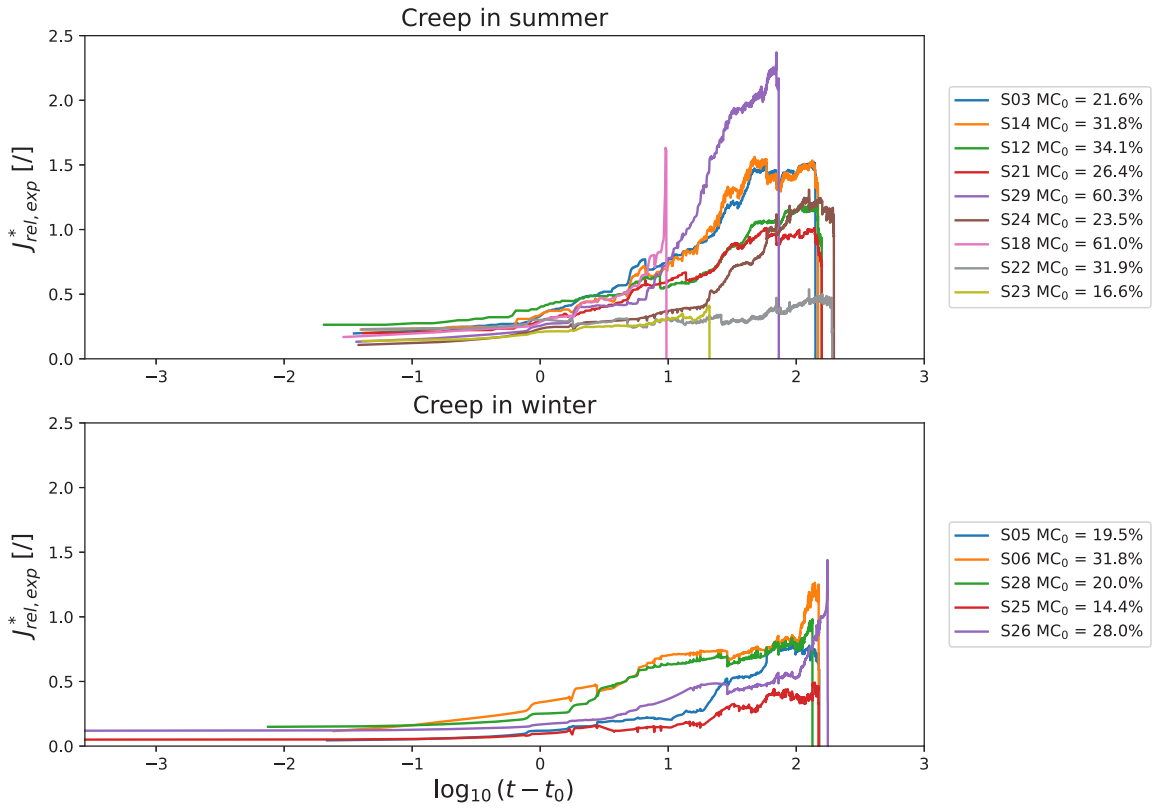

Fig. 12. Relative compliance J^*_{rel} as a function of time for creep tests in summer and in winter. Initial moisture content MC_0 and beam number S_{ij} are indicated. (For interpretation of the references to colour in this figure legend, the reader is referred to the web version of this article.)

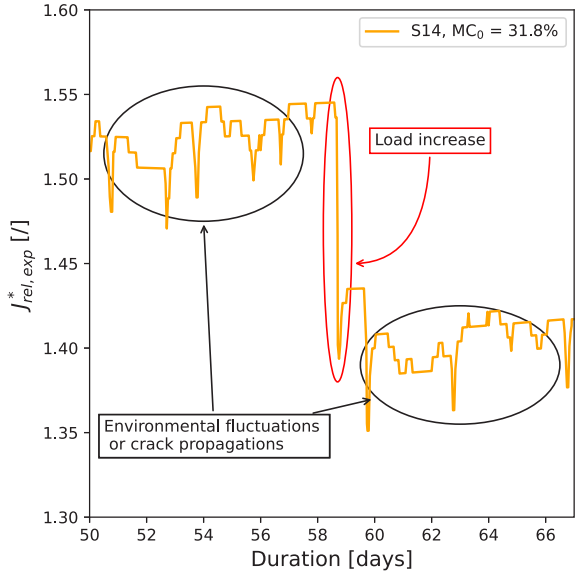

Fig. 13. Focus on $J^*_{rel,exp}$ fluctuation moment of S14. A load increase is identified and others are attributed to environmental fluctuations or crack propagation.

where $t^-_{\Delta\sigma_1}$ and $t^+_{\Delta\sigma_1}$ are respectively the times right before and right after the load increase. For an elastic response, Eq. (9) becomes:

$$\frac{\epsilon_0 + \Delta\epsilon_1}{\Delta\sigma_0 + \Delta\sigma_1} \approx \frac{\epsilon_0}{\Delta\sigma_0} \tag{9}$$

leading to Eq. (10):

$$J^*(t^-_{\Delta\sigma_1}) = \frac{\epsilon_0 + \epsilon_t}{\Delta\sigma_0} > J^*(t^+_{\Delta\sigma_1}) = \frac{\epsilon_0}{\Delta\sigma_0} + \frac{\epsilon_t}{\Delta\sigma_0 + \Delta\sigma_1} \tag{10}$$

3.3. Crack trajectories

After the tests, observations of fracture facies were made. All crack propagations occurred through rising towards the compression zone, whatever the grain angle is Figs. 14(a) and 14(b)), though it was assumed that crack follows the grain. Crack slope varies from 3% to 10%, as shown in Fig. 14(c).

4. Discussion

4.1. Estimation of the real compliance

In order to access the real $J(t)$ that defines creep evolution, it can be modelled as if it evolves linearly with $\log(t)$, where t represents the duration of the test. It leads to a modelled J_m written in Eq. (11) as:

$$J_m(t) = J_0 \left[1 + max\left(\beta \log\left(\frac{t}{\alpha}\right), 0\right)\right] \tag{11}$$

where β is the slope of the linear evolution with $\log(t)$, and α is the time at which creep starts. Such compliance function is in line with observations of long-term trends [32]. α and β can be determined by fitting J^*_m (Eq. (12)) on J^*_{exp} as:

$$J^*_m(t) = \frac{\epsilon_m(t)}{\sigma(t)} = \frac{\sum_{i=0}^{N} \Delta\sigma_i . J_m(t - t_i)}{\sum_{i=0}^{N} \Delta\sigma_i} \tag{12}$$

Once α and β are determined, an expression of relative creep can be obtained as $J_{m,rel} = \beta \log(t/\alpha)$. The maximum value of $J_{m,rel}$ reached before failure can be compared to the so-called k_{def} for structural serviceability design. α and β are fitted using Nelder–Mead algorithm implemented in scipy module of Python, where the root mean square between J^*_m and J^*_{exp} is minimised. For beam S03, the results of experimental and modelled J^* time-evolution are plotted in Fig. 15(a), and the relative creep $J_{m,rel}$ in Fig. 15(b). α and β are illustrated in

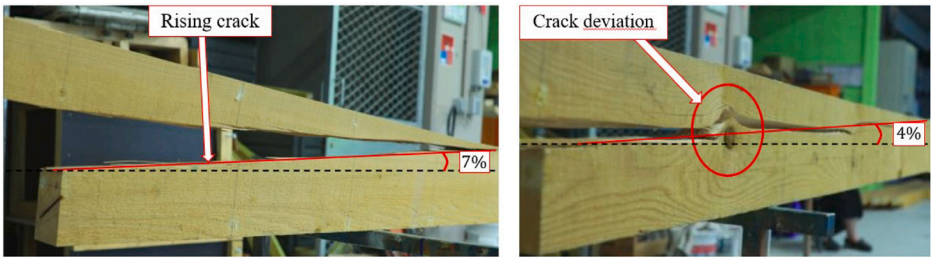

(a) Crack slope of beam S14. (b) Crack slope of beam S05.

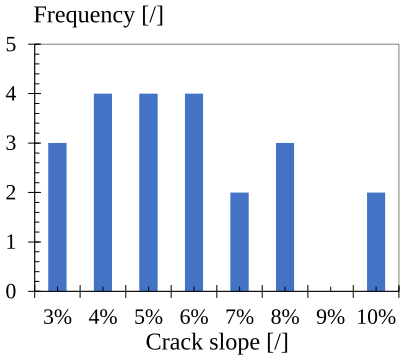

(c) Crack slopes after failure.

Fig. 14. Observations of rising crack propagations.

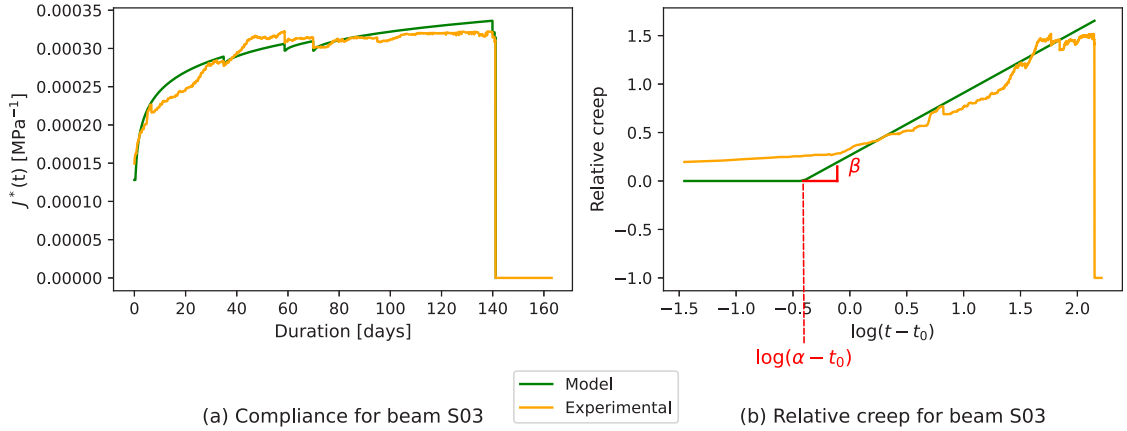

(a) Compliance for beam S03 (b) Relative creep for beam S03

Fig. 15. Comparison between the experimental and modelled J^* and k_{def} for beam S03 loaded in summer. (For interpretation of the references to colour in this figure legend, the reader is referred to the web version of this article.)

the Figure. Though $J^*_{rel,exp}$ corresponds to an underestimated $J_{m,rel}$ (Inequality (6)), it is plotted in Fig. 15(b) for comparison. The optimised α and β are plotted as functions of E^d_S for all beams, the creep season being indicated by the colour, see Fig. 16.

As α represents the time at which the compliance starts to increase, it is consistent that most of the highest values were reached in winter. Similarly, as β represents a creep speed it is consistent that the highest values were reached in summer. Sun exposure are added as it might have had an impact but no significant tendency can be observed. Finally, no correlation is observed between β and E^d_S. Indeed as E^d_S is affected by the grain angle and the micro-fibril angle, it could have affected the creep speed too.

The relative compliance reached at the end of the test is given in Fig. 17 as a function of the initial moisture content MC_0. The results show no relevant correlation (adjusted $R^2 = 0.1$), though the greenest beams should have reached a higher $J_{m,rel}$. As comparison, k_{def} from Eurocode 5 is fixed at 2 for dry wood in outdoor environment and 3 if wood is loaded in green state. In these experiments, the estimated $J_{m,rel}$ never reached 3 and almost always stayed below 2, the +1 increase for wood above 20% of initial MC seeming excessive.

4.2. Contribution of fracture to deflection

Considering the constant function $f_{uncrack}$ relating $U_{c,exp}$ and J^*_{exp} for uncracked notched beam, an estimated A_{crack} can be stated, as shown in Eq. (13):

$$A_{crack}(t) = 1 - \frac{f_{uncrack}}{f_{crack}(t)} \tag{13}$$

where $A_{crack}(t)$ is the percentage of the observed deflection that is explained by the f_{crack} function evolution. It is an estimation of a deflection only involved by crack. Such $A_{crack}(t)$ is plotted as a function

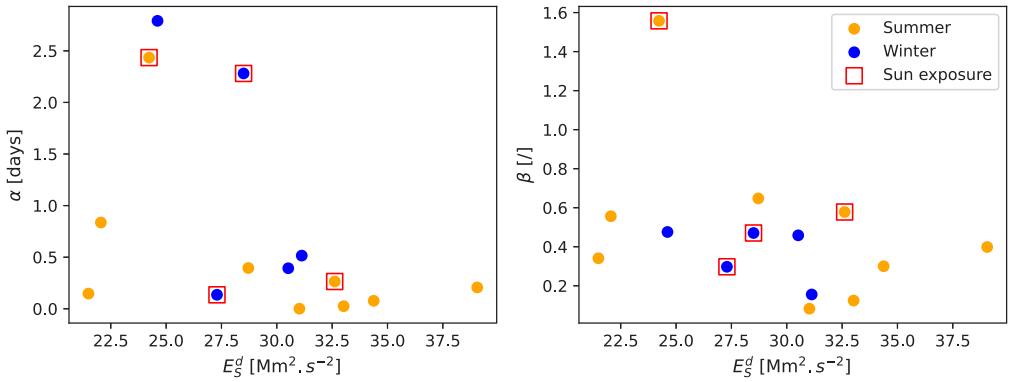

(a) α: Creep start (b) β: Creep log rate

Fig. 16. Results of the optimised α and β as functions of the basic specific modulus E_S^d. (For interpretation of the references to colour in this figure legend, the reader is referred to the web version of this article.)

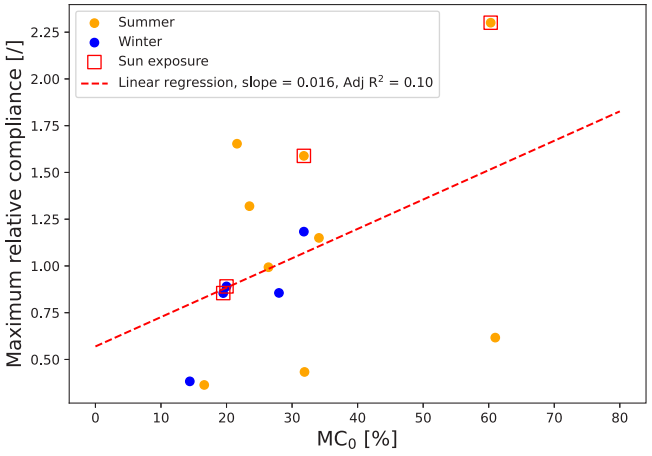

Fig. 17. Maximum relative compliance $J_{m,rel}$ as a function of initial moisture content MC_0. Season and sun exposure are specified with their respective colour. Linear regression is added with its slope and adjusted coefficient of determination (Adj R^2). (For interpretation of the references to colour in this figure legend, the reader is referred to the web version of this article.)

of time in Fig. 18. $A_{crack}(t)$ varies from 1 to 13%, reaching its maximum value for beams loaded in winter as viscoelastic deflection is lower for that season. Although assumptions are strong in that computation it can be concluded that crack has a lower impact than creep on the total deflection.

4.3. Crack opening comparison

It is possible to evaluate the crack opening using the beam deflection function, based on geometrical supposition. Considering a deflected and cracked beam, when the crack propagates the part that comes off keeps the same deflection slope as that of the crack tip, see Fig. 19. Then, it comes that crack opening can be estimated by Eq. (14):

$$\begin{cases} C_{Ol} = u(L_N + C_{Ll}) - u(L_N) - C_{Ll} \times \frac{du}{dx}(L_N + C_{Ll}) \\ C_{Or} = u(L - L_N - C_{Lr}) - u(L - L_N) - C_{Lr} \times \frac{du}{dx}(L - L_N - C_{Lr}) \end{cases} \tag{14}$$

That can be written:

$$\begin{cases} C_{Ol} = \Delta u_l - C_{Ll} \times u'(L_N + C_{Ll}) \\ C_{Or} = \Delta u_r - C_{Lr} \times u'(L - L_N - C_{Lr}) \end{cases} \tag{15}$$

where L_N is the notch length; Δu_l and Δu_r are the differences between deflection at the crack tip and at the notch (positive difference), to the left and to the right respectively; u' is the deflection derivative function with respect to x (du/dx). Without crack propagation, the crack tip is coincident with the notch when $\Delta u = 0$ and $C_L = 0$, consistently leading to $C_O = 0$.

In Fig. 19 the vertical displacements have been amplified for the purpose of clarity; in reality they are sufficiently small, so that initial and final configurations can be assumed identical. Some typical crack opening results are plotted in Fig. 20.

$C_{O,exp}$ corresponds to the experimental results of the crack opening, and $C_{O,c}$ uses shrinkage-swelling measurements ΔH to correct $C_{O,exp}$ such as Eq. (16):

$$C_{O,c}(t) = C_{O,exp}(t) + C_{O,exp}(t=0) \times \frac{\Delta H(t)}{H_0} \tag{16}$$

with H_0 the initial beam's height. $C_{O,fd}$ is the finite difference crack opening computed with Eq. (15). The measured $C_{O,exp}$ is caused by different phenomena, while only shrinkage-swelling and the geometrical effect of beam theory (Fig. 19) are taken into account in $C_{O,fd}$. A good fitting is obtained in only one case (Fig. 20(a)), while it is bad for all other beams (examples in Figs. 20(b) and (c)). This can be explained by the occurrence of non-linear fracture mechanics in the crack tip region, differences between the two faces measured, or complex 3D cracking patterns incompletely described by the average position of crack tips on both faces.

4.4. Rising cracks

Taking an energetic approach, as it is common in linear fracture mechanics, reasons that may explain systematic rising crack propagations are given as follows:

1. Softwoods have an overlapping of tracheids [9] that may allow a crack to rise slightly with no additional energetic cost, as shown in Fig. 21. Supposing that on average, overlap is at half-length of the tracheids, and it explains $D_{trach}/(L_{trach}/2) = 2\%$ of slope.
2. A rising crack is what maximises the work of external forces as it maximises the beam's deflection. Although fracture toughness is minimum along the grain, a rising crack is an optimisation between maximising the work of external forces and minimising the fracture toughness, the outcome not being a horizontal crack.

5. Conclusions

This paper presents the results of an experimental campaign on full-scale notched beams of silver fir wood. The studied beam's batch had firstly been characterised by vibration tests and basic-density measurements, showing its mechanical properties distribution. Then ramp-loading bending tests and bending creep tests in outdoor conditions

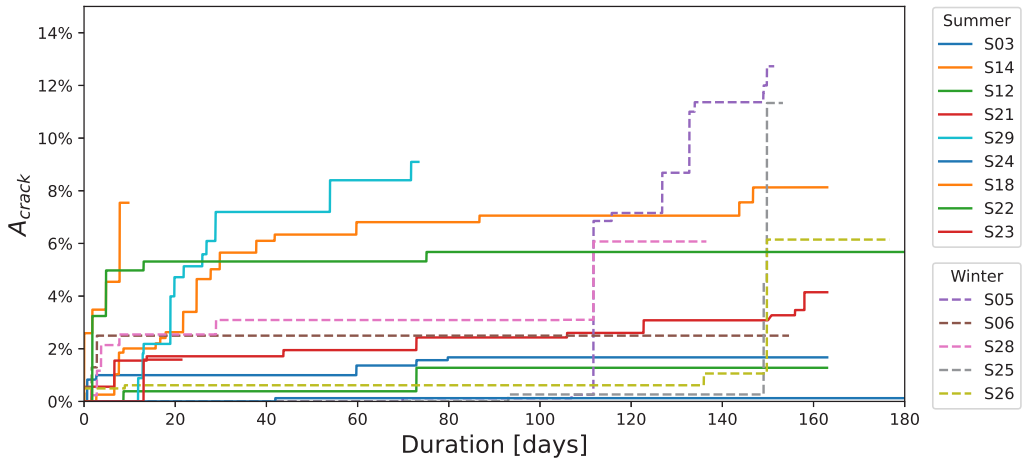

Fig. 18. Percentages of the observed deflections explained by crack as a function of time for all creep tests. (For interpretation of the references to colour in this figure legend, the reader is referred to the web version of this article.)

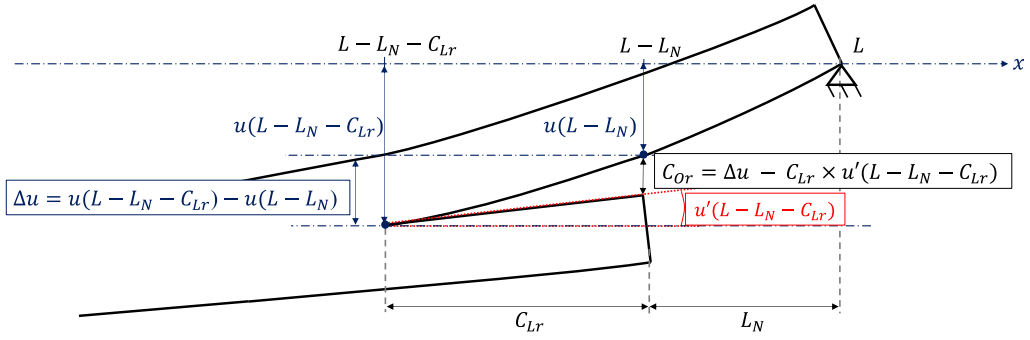

Fig. 19. Excessively deflected beam with crack on right side, schematically showing C_O geometrical estimation. u and u' represent the deflection and rotation function, respectively.

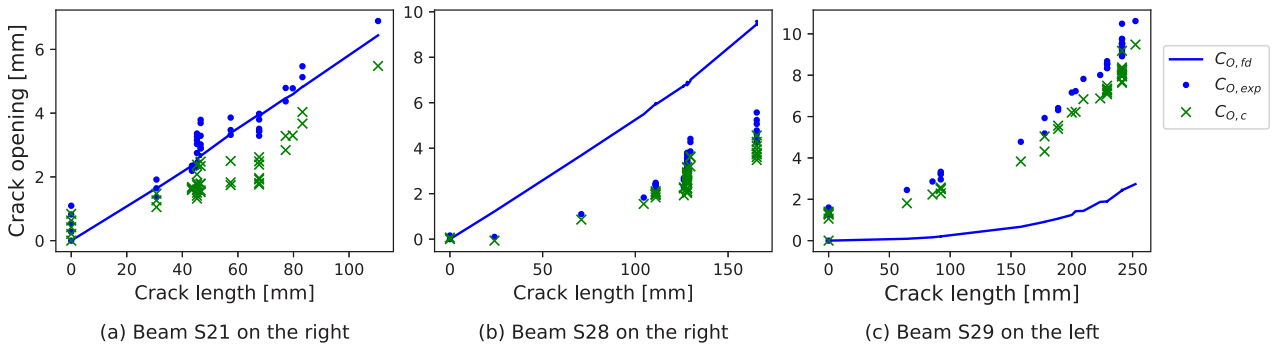

Fig. 20. Experimental crack opening ($C_{O,exp}$), corrected crack opening ($C_{O,c}$) and numerical crack opening computed with Eq. (15) ($C_{O,fd}$) as a function of the associated crack length for three beams.

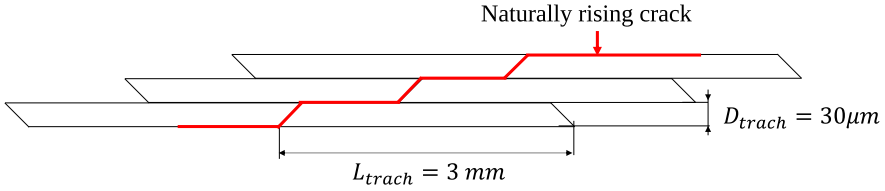

Fig. 21. Anatomical explanation for a naturally rising crack propagation.

were carried out on wood at different initial MCs, including green wood. Comparison between dynamic and static compliances shows a high difference but with a consistent hierarchy, explained by tests conditions. All other things being equal, initial MC has no visible impact on instantaneous maximum force. The dynamic compliance seems proportional to that maximum force, and observations suggest that it is

explained by the dowelling effect. The central deflection measurements in multi-step creep tests does not allows to compute the real compliance J_{exp}, that is thus approximated using linear evolution with the logarithm of time. The parameters needed for that approximation, α and β, are fitted in order to comply with experimental results. The maximum value of the modelled relative compliance show no correlation with the initial MC. Furthermore, it never reaches the k_{def} proposed by Eurocode 5 in that situation, suggesting oversizing for green wood. The Euler–Bernoulli bending equation resolution taking crack propagation into account allows to estimate that the total deflection is mainly due to creep instead of crack. The numerical crack opening derived with geometrical assumptions and beam theory was most of time not sufficient to explain the experimental crack opening measured, even corrected with shrinkage-swelling measurements. Indeed, beam theory is not adapted to fracture mechanics analysis and does not take into account non-linear effect and 3D problems. Finally, it is observed that crack trajectories are always rising towards the compression zone, whatever the grain angle is, from 3 to 10% of slope. Two possible explanations for this phenomenon are described: tracheids overlapping and energy optimisation.

6. Perspectives

This study opens many new perspectives, some of which are proposed below.

1. Determining the fracture properties of silver fir at different initial moisture contents. Such data would help analyse the results in Fig. 17 and explaining rising crack trajectories.
2. Realise crack tests where applied-load is not orthogonal to the grain and measure the crack direction. Furthermore, undergo microscopical observations of fracture facies in order to observe the anatomical crack path.
3. New ramp-loading tests with full-field measurements. This would allow to have several crack measurements with high precision and no shrinkage-swelling disturbances. The numerical and experimental crack openings could then be fairly compared.
4. Developping a rheological model would allow to take viscoelasticity into account in the compliance computation. It would enhance greatly the results accuracy as shown in Fig. 12.

CRediT authorship contribution statement

Arthur Bontemps: Writing – original draft, Methodology, Investigation, Formal analysis, Data curation, Conceptualization. **Rostand Moutou Pitti:** Validation, Supervision, Resources, Project administration, Funding acquisition. **Eric Fournely:** Writing – review & editing, Validation, Supervision. **Gaël Godi:** Supervision, Resources, Methodology, Data curation. **Joseph Gril:** Writing – review & editing, Visualization, Validation, Supervision, Methodology, Investigation, Funding acquisition, Formal analysis, Conceptualization.

Declaration of competing interest

The authors declare that they have no known competing financial interests or personal relationships that could have appeared to influence the work reported in this paper.

Data availability

Data will be made available on request.

Acknowledgements

The authors would like to thank the Auvergne Rhône-Alpes region for the Ph.D. scholarship as well as the fundings of the Hub-Innovergne program of the Clermont Auvergne University, France.

Compliance with ethical standards

On behalf of all authors, the corresponding author states that there is no conflict of interest.

Appendix. Euler–Bernoulli bending equation resolved using finite difference method

In beam theory, the deflection is derived from the Euler–Bernoulli bending equation, i.e. Eq. (A.1):

$$\frac{d^2u}{dx^2} = J \times \frac{M_z(x)}{I_z} \tag{A.1}$$

where J is the compliance, I_z and $M_z(x)$ are respectively the second moment of inertia and the bending moment bout the z axis, u is the deflection and x the beam's axis.

Based on Fig. 7, two Dirichlet boundary conditions can be defined by Eq. (A.2):

$$\begin{aligned} u(0) &= u_0 = 0 \\ u(L) &= u_N = 0 \end{aligned} \tag{A.2}$$

Considering the three-point centered scheme such as Eq. (A.3):

$$\frac{u_{i-1} - 2u_i + u_{i+1}}{\Delta x^2} = \left(\frac{M_z}{I_z}\right)_i \times J \tag{A.3}$$

The boundary conditions can be written by Eq. (A.4):

$$\begin{aligned} \frac{-2u_1 + u_2}{\Delta x^2} &= \left(\frac{M_z}{I_z}\right)_1 \times J \\ \frac{u_{N-2} - 2u_{N-1}}{\Delta x^2} &= \left(\frac{M_z}{I_z}\right)_{N-1} \times J \end{aligned} \tag{A.4}$$

If equations are collected into a matrix system, it leads to Eq. (A.5):

$$\frac{1}{\Delta x^2} . \underline{\underline{A}} . \underline{u}_{fd} = \underline{b} . J \tag{A.5}$$

where:

$$\underline{\underline{A}} = \begin{bmatrix} -2 & 1 & 0 & \dots & & & & & \\ 1 & -2 & 1 & 0 & \dots & & & & \\ 0 & 1 & -2 & 1 & 0 & \dots & & & \\ & & & & \ddots & & & & \\ & & & & & 0 & 1 & -2 & 1 \\ & & & & & 0 & 0 & 1 & -2 \end{bmatrix}_{(N-1)\times(N-1)} \tag{A.6}$$

$$\underline{b} = \begin{bmatrix} (M_z/I_z)_1 & (M_z/I_z)_2 & . & . & . & (M_z/I_z)_{N-2} & (M_z/I_z)_{N-1} \end{bmatrix}_{(N-1)} \tag{A.7}$$

$$\underline{u}_{fd} = \begin{bmatrix} u_1 & u_2 & . & . & . & u_{N-2} & u_{N-1} \end{bmatrix}_{(N-1)} \tag{A.8}$$

The system to be resolved can finally be summarised by Eq. (A.9):

$$\underline{u}_{fd} = \underline{\underline{A}}^{-1} . \underline{b} \times \Delta x^2 . J \tag{A.9}$$

The central deflection computed with FDM is therefore $U_{c,fd} = \underline{u}_{fd}[(N-1)/2]$ with an even N.

References

[1] FCBA, Memento de la Filière Bois, Tech. Rep., FCBA, 2020.
[2] L. Martin, H. Cochard, S. Mayr, E. Badel, Using electrical resistivity tomography to detect wetwood and estimate moisture content in silver fir (Abies alba Mill.), Ann. Forest Sci. 78 (3) (2021) 1–17, http://dx.doi.org/10.1007/s13595-021-01078-9, number: 3 Publisher: BioMed Central.
[3] AFNOR, NF EN 1995-1-1. Eurocode 5 - Conception et calcul des structures en bois - Partie 1-1 : généralités - Règles communes et règles pour les bâtiments, 2004.
[4] L.D. Armstrong, R.S.T. Kingston, Effect of moisture changes on creep in wood, Nature 185 (4716) (1960) 862–863, http://dx.doi.org/10.1038/185862c0, number: 4716 Publisher: Nature Publishing Group.

[5] S.M. Holzer, J.R. Loferski, D.A. Dillard, A review of creep in wood: Concepts relevant to develop long-term behavior predictions for wood structures, Wood Fiber Sci. (1989) 376–392, URL https://wfs.swst.org/index.php/wfs/article/view/1389.
[6] D.G. Hunt, J. Gril, Evidence of a physical ageing phenomenon in wood, J. Mater. Sci. Lett. 15 (1) (1996) 80–82, http://dx.doi.org/10.1007/BF01855620.
[7] M. Mislav, P. Stjepan, K. Miljenko, O.C. Anka, S. Nikola, P. Slivana, Factors influencing behaviour of solid wood bending process, Drvna Ind. 74 (2023) http://dx.doi.org/10.5552/drvind.2023.0020.
[8] P. Perré, O. Aguiar, Fluage du bois vert à haute température (120 °C), Ann. Forest Sci. 56 (5) (1999) 403–416, http://dx.doi.org/10.1051/forest:19990505, URL http://www.afs-journal.org/10.1051/forest:19990505.
[9] M.-C. Trouy, P. Triboulot, Matériau bois - Structure et caractéristiques, Tech. l'Ingén. (2019) 41.
[10] T.-Y. Hsieh, Structure Properties Relationships that Lead to Delayed Wood Behaviour : From Understanding Mechanisms to Determining Predictive Indicators (These de doctorat), Université de Montpellier, 2022, (2022-....). URL https://www.theses.fr/2022UMONS092.
[11] J. Dlouhá, B. Clair, O. Arnould, P. Horáček, J. Gril, On the time–temperature equivalency in green wood: Characterisation of viscoelastic properties in longitudinal direction, Holzforschung 63 (3) (2009) 327–333, http://dx.doi.org/10.1515/HF.2009.059, publisher: De Gruyter Section: Holzforschung.
[12] G. Pot, E. Toussaint, C. Catherine, Viscoelastic behaviour of maturating green poplar wood, in: Conference Proceedings of the Society for Experimental Mechanics Series 1, 2013.
[13] C. Montero, J. Gril, Comparison Between Wood Hygromechanical Description and Deformation Modification Factors of Eurocode 5, 2016, p. 6, URL https://hal.science/hal-01352723.
[14] T.y. Hsieh, F.-C. Chang, Effects of moisture content and temperature on wood creep, Holzforschung 72 (2018) http://dx.doi.org/10.1515/hf-2018-0056.
[15] R. Jockwer, Structural Behaviour of Glued Laminated Timber Beams with Unreinforced and Reinforced Notches (Doctoral Thesis), ETH Zurich, 2014, http://dx.doi.org/10.3929/ethz-a-010171641, accepted: 2017-12-20T13:43:33Z.
[16] C.F. Pambou Nziengui, R. Moutou Pitti, E. Fournely, J. Gril, G. Godi, S. Ikogou, Notched-beam creep of Douglas fir and white fir in outdoor conditions: Experimental study, Constr. Build. Mater. 196 (2019) 659–671, http://dx.doi.org/10.1016/j.conbuildmat.2018.11.139.
[17] Gustafsson, A study of strength of notched beams, in: International Council for Research and Innovation in Building and Construction, Working Commission W18 - Timber Structures, 1998.
[18] R. Jockwer, R. Steiger, A. Frangi, State of the art review of approaches for the design of timber beams with notches, J. Struct. Eng. 140 (3) (2014) 04013068, http://dx.doi.org/10.1061/(ASCE)ST.1943-541X.0000838, publisher: American Society of Civil Engineers.
[19] L. Brancheriau, Expertise Mécanique des Sciages par Analyses des Vibrations Dans le Domaine Acoustique (phdthesis), Université de la Méditerranée - Aix-Marseille II, 2002.
[20] JCSS, Joint Committee on Structural Safety Probabilistic Model Code. Part 3 : Resistance Models, Tech. Rep., JCSS, 2006.
[21] CIRAD, Fiche TROPIX 7 Abies alba, 2012.
[22] B. Thibaut, J. Gril, Tree growth forces and wood properties, Peer Community J. 1 (2021) http://dx.doi.org/10.24072/pcjournal.48.
[23] A. Billard, R. Bauer, F. Mothe, F. Colin, F. Longuetaud, Wood density variations between tree components should be considered to correctly estimate tree biomass available for fifferent uses, HAL - Arch. Ouverts (2019).
[24] A. Matar, The Mechano Sorptive Creep of Softwood in Bending (Ph.D), South Bank University, 2003, accepted: 2003.
[25] AFNOR, NF EN 408+A1 - Structures en bois, in: Bois de Structure et Bois Lamellé-Collé, 2012.
[26] A. Bontemps, G. Godi, E. Fournely, R. Moutou-Pitti, J. Gril, Implementation of an optical measurement method for monitoring mechanical behaviour, Exp. Tech. (2023) http://dx.doi.org/10.1007/s40799-023-00636-2.
[27] F.F.P. Kollmann, W.A. Côté, Principles of Wood Science and Technology: I Solid Wood, Springer, Berlin, Heidelberg, 1968, http://dx.doi.org/10.1007/978-3-642-87928-9, URL https://link.springer.com/10.1007/978-3-642-87928-9.
[28] D.G. Hunt, Linearity and non-linearity in mechano-sorptive creep of softwood in compression and bending, Wood Sci. Technol. 23 (4) (1989) 323–333, http://dx.doi.org/10.1007/BF00353248.
[29] AFNOR, NF EN 338, in: Bois de Structure - Classes de Résistance, 2016.
[30] D. Guitard, Mécanique du Matériau Bois et Composites, Collection Nabla, Librairie Eyroles, 1987.
[31] L. Brancheriau, Caractérisation Acoustique et Ultrasonore des Produits Bois et Composites (thesis), UM2, 2013.
[32] D.G. Hunt, A unified approach to creep of wood, Proc. R. Soc. Lond. Ser. A Math. Phys. Eng. Sci. 455 (1991) (1999) 4077–4095, http://dx.doi.org/10.1098/rspa.1999.0491, publisher: Royal Society.